

Induction Motor Bearing Faults Diagnosis Using Stator Current and Vibration Analysis

Mohamed Boudiaf Koura^{1*}, Ahmed Hamida Boudinar¹, Ameer Fethi Aimer¹,
Mohammed-el-Amine Khodja¹

¹ Department of Electrotechnics, Faculty of Electrical Engineering, Laboratory of Development of Electric Drives, University of Sciences and Technology of Oran - Mohamed Boudiaf (USTO-MB), 31000 Oran, Al Mnaouar, P. O. B. 1505, Algeria

* Corresponding author, e-mail: mohamedboudiaf.koura@univ-usto.dz

Received: 30 September 2020, Accepted: 18 November 2020, Published online: 04 October 2021

Abstract

Several researches claim that the vibration technique, widely used in industry, is more efficient compared to the stator current analysis in the diagnosis of mechanical faults. On the other hand, researches show that the current technique is more advantageous especially in the diagnosis of electrical faults, in addition to the simplicity of the sensor positioning. The aim of this paper is to show that both diagnosis techniques can be complementary. For this, a comparative analysis of both diagnosis techniques performances is achieved. To this end, fault diagnosis of rolling element bearings used in induction motors is taken as an example, given the importance of bearings in energy transfer. Experimental results obtained show the complementarity of both techniques and their performances according to the faulty element of bearings.

Keywords

diagnosis, induction motor, bearing fault, vibration, stator current

1 Introduction

Rolling element bearings, as an electromechanical interface, allow the energy conversion in induction motors, which makes them more fragile [1]. Indeed, several statistical studies [1–3] have shown that failures due to bearings represent 40 % to 69 % of total failures depending on the motors power range. Fig. 1 shows the distribution of various faults affecting the induction motor.

It is therefore logical, from an industrial, scientific and financial point of view, to concentrate efforts of detection and diagnosis of induction motors on rolling element bearing faults. This diagnosis preserves the safety of personnel, avoids stopping the entire production line, which increases the lifetime of these motors and minimizes financial losses.

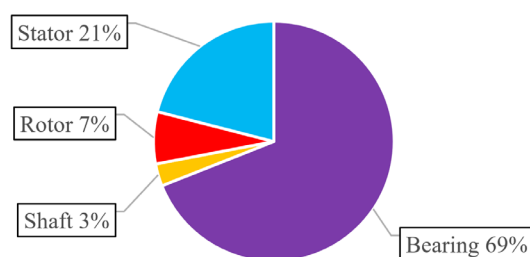


Fig. 1 Distribution of various faults affecting induction motors

In this context, vibration analysis is the most used technique in industry because it can detect most mechanical faults and more precisely bearing faults. However, the major drawback of this technique is the need for access to the motor body to position the vibration sensor. In addition, the assembly of these sensors requires competent personnel to have reliable measurements. Furthermore, this technique can only be used to diagnose large units working on critical and sensitive processes given the cost of this sensor. Finally, note that the reliability of this technique can be biased by the presence of abnormal vibrations due, for example, to attachment's problems of the motor [4–7].

Another technique based on the stator current analysis for bearing faults diagnosis called Motor Current Signature Analysis (MCSA) [8–12]. This technique has several advantages such as: an easy installation of the current sensor which does not require access to the body of the motor as well as the obtained information from the current spectrum about the state of the motor and the different types of faults. This technique is widely used in the diagnosis of electrical faults, but unfortunately remains less used for mechanical faults diagnosis.

Several researches [13–15] have shown that the presence of a bearing fault is highlighted by the appearance of a specific frequency signature on both vibration and current spectrums but at different frequency bands. To identify this frequency signature characterizing the bearing fault from vibration or current, the estimation of the Power Spectral Density (PSD) by Periodogram is the most used method in industry because it presents an easy programming and a fast execution due to the use of the Fast Fourier Transform (FFT) algorithm.

The aim of this paper is to compare the performances and capacities of both aforementioned techniques, vibration and stator current techniques. This comparison is made on the basis of experimental tests carried out on faulty bearings. To this end, the performances of both techniques are illustrated by the analysis of the measured signals using the PSD estimation by Periodogram.

2 Bearing fault signatures

Rolling element bearing is one of the most important components of electric motors. Bearings mainly consists of an outer race, an inner race, balls and a cage which ensures equidistance between balls as shown in Fig. 2 [16–18].

Where B_D and C_D are respectively the ball and the cage diameters, β the contact angle and N_b the number of balls.

Unfortunately, due to corrosion, improper installation, or poor lubrication, this bearing can suffer from certain failures of its components. The failure of these elements is manifested by the appearance of frequency signatures on the vibration and current signals.

2.1 Vibrational frequency signatures of bearing fault

The failure of each bearing's element is manifested by vibrations in the induction motor. Several studies [16–18] have shown that each faulty element is characterized by a specific frequency signature as shown by Eqs. (1) to (5):

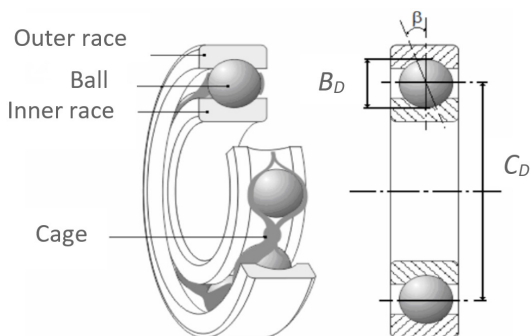


Fig. 2 Geometry of rolling element bearings

- Outer race fault:

$$f_{\text{outer,race}} = \frac{N_b}{2} f_r \left(1 - \frac{B_D}{C_D} \cos \beta \right) \quad (1)$$

- Inner race fault:

$$f_{\text{inner,race}} = \frac{N_b}{2} f_r \left(1 + \frac{B_D}{C_D} \cos \beta \right) \quad (2)$$

- Cage fault:

$$f_{\text{cage}} = \frac{1}{2} f_r \left(1 - \frac{B_D}{C_D} \cos \beta \right) \quad (3)$$

- Ball fault:

$$f_{\text{ball}} = \frac{C_D}{B_D} f_r \left(1 - \frac{B_D^2}{C_D^2} \cos^2 \beta \right). \quad (4)$$

The f_r is the rotor frequency which can be deduced from the mechanical speed of the induction motor n_r . This relationship is defined from:

$$f_r = \frac{n_r}{60}. \quad (5)$$

2.2 Electrical frequency signatures of bearing faults

All motor vibrations caused by mechanical faults such as bearing faults are manifested by both amplitude and phase modulation in the stator current. This modulation obviously affects the current spectrum by the appearance of frequency components around the fundamental as shown in Eq. (6) [19, 20]:

$$f_{\text{bear}} \text{ (Hz)} = |f_s \pm k \times f_v| \quad k = 1, 2, 3 \dots \quad (6)$$

where f_s is the supply frequency. f_v is one of the vibrational frequencies characterizing the faulty element defined by Eqs. (1), (2), (3) and (4) i.e.: $f_{\text{outer,race}}$, $f_{\text{inner,race}}$, f_{cage} and f_{ball} .

3 Identification of bearing faults using periodogram technique

Among the frequency analysis methods for identifying the bearing's faulty element, the estimation of the Power Spectral Density (PSD) using the Periodogram technique is chosen. This method is widely used in industry because it is [11, 17]:

- Independent of the physical nature of the signal $x(t)$ to be processed (vibration or electric), provided the signal is stationary.

- Easy to program.
- Fast due to the use of the FFT (Fast Fourier Transform) algorithm.
- Easy to implement on FPGA-based cards for real-time applications.

The estimation of the PSD by Periodogram is defined as being the square of the module of the Fourier Transform of the digital signal to be processed $x(n)$, as shown in Eq. (7) [11, 15, 21]:

$$PSD(k\Delta f) = \frac{\left| \sum_{n=0}^{N-1} x(n) \times e^{-j2\pi nk\Delta f} \right|^2}{N} \quad (7)$$

where Δf is the frequency resolution defined as follows:

$$\Delta f = \frac{F_{sp}}{N} \quad (8)$$

where F_{sp} is the sampling frequency and N is the number of samples in the digitized signal.

Note that to improve the frequency resolution, it is advisable to increase the acquisition time, in other words the number of samples. Unfortunately, this can affect the computation time.

4 Experimental results

4.1 Experimental setup description

The motor used in our experimental tests is a three-phase squirrel cage induction motor, its parameters are: 3 kW; 50 Hz; 7 A; 1410 rpm. This motor is coupled to a Direct Current generator connected to a resistive load. The measurement bench used is illustrated by Fig. 3.

Two measurement lines are used at the same time for the acquisition of both signals to be processed:

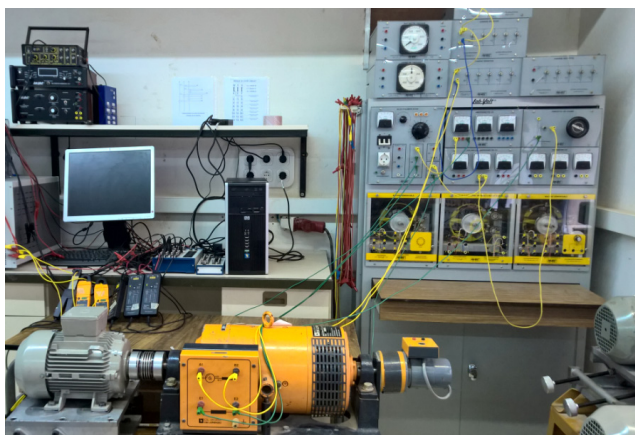


Fig. 3 Experimental setup description

- For the vibration signal: a piezoelectric triaxial accelerometer (CTC: AC230-1D) with integrated electronics IEPE (Integrated Electronic Piezo-Electric) is used to measure the motor vibration along the three axes X, Y, Z. Fig. 4 shows the positioning of the vibration sensor on the motor.
- For the electrical signal: three Hall-effect current sensors (Fluke i30s) are used to measure the three stator currents. Fig. 5 shows the positioning of the current sensor regarding the induction motor.

All signals (vibration and stator current) are digitized at the same time using a NI USB-6229 acquisition card with 08 inputs. Both measurement lines are managed by a computer which also allows the processing of the acquired signals. All acquisitions were made in steady state with a rotation speed of 1440 rpm, corresponding to a rotation frequency of 24 Hz. The acquisition parameters chosen are respectively: an acquisition time of 20 seconds and a sampling frequency of 10 KHz. Under these conditions, we obtain a frequency resolution equal to 0.05 Hz. To have a more reliable analysis because of the random nature of the measured signals, several acquisitions were made for each operating mode.



Fig. 4 Positioning of the vibration sensor



Fig. 5 Positioning of the current sensors

The rolling element bearings analyzed in this paper (opposite side of the coupling) is 6205-ZZ bearing. The geometric parameters of this bearing are given in the Appendix. The studied faults are created artificially by the EDM (Electrical Discharge Machining) technique, with the aim of recreating the same situations as those of real faults. Fig. 6 illustrates the fault created in bearings used in our experimental tests.

Operating modes carried out in this study are:

- Motor operating with healthy bearing.
- Motor operating with an outer race fault.
- Motor operating with an inner race fault.
- Motor operating with a cage fault.

According to the theoretical study, the frequency signatures of bearing faults corresponding to the faulty operating modes, are likely to appear at some frequencies according to:

- The geometric characteristics of the analyzed bearing.
- Equations (1), (2), (3) for the vibration technique.
- Equations (1), (2), (3) and (5) for the current technique.

Knowing these frequency signatures, the analysis can be carried out only on specific frequency bands according to the searched fault. These frequency bands are given in Table 1.

4.2 Motor operating with healthy bearings

In this operating mode, acquired signals are analyzed assuming that both bearings (coupling side and opposite

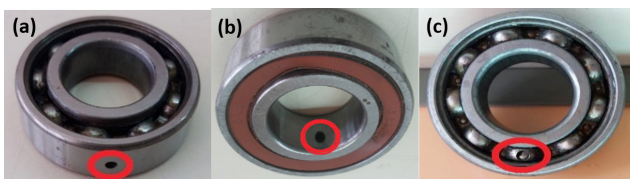


Fig. 6 Bearing faults: (a) Outer race fault, (b) Inner race fault, (c) Cage fault

Table 1 Frequency bands for both techniques: vibration and current

Bearing fault		Fault signature and Frequency band	
		Vibration technique	Current technique
Outer race fault	Fault signature	85.73 Hz	35.73 Hz
	Frequency band	[80 Hz–90 Hz]	[30 Hz–40 Hz]
Inner race fault	Fault signature	130.26 Hz	80.26 Hz
	Frequency band	[125 Hz–135 Hz]	[75 Hz–85 Hz]
Cage fault	Fault signature	9.52 Hz	40.48 Hz
	Frequency band	[5 Hz–15 Hz]	[35 Hz–45 Hz]

side of the coupling) have no apparent fault. Figs. 7 and 8 illustrate the vibration and current spectrum for this operating mode according to the frequency analysis bands determined in Table 1.

- For the vibration technique: according to Fig. 7, the spectral analysis of the vibration signals obtained by estimation of the PSD using the Periodogram technique, detects the following frequency signatures (85.85 Hz / -60.85 dB and 129.4 Hz / -62.24 dB) on both frequency bands [80 Hz–90 Hz] and [125 Hz–135 Hz] respectively. It is assumed that these frequencies represent the signatures of the inner race and outer race faults, according to Table 1. The presence of these frequencies is certainly due to the scratches caused by the assembly and disassembly operation of bearings. On the other hand, no signature

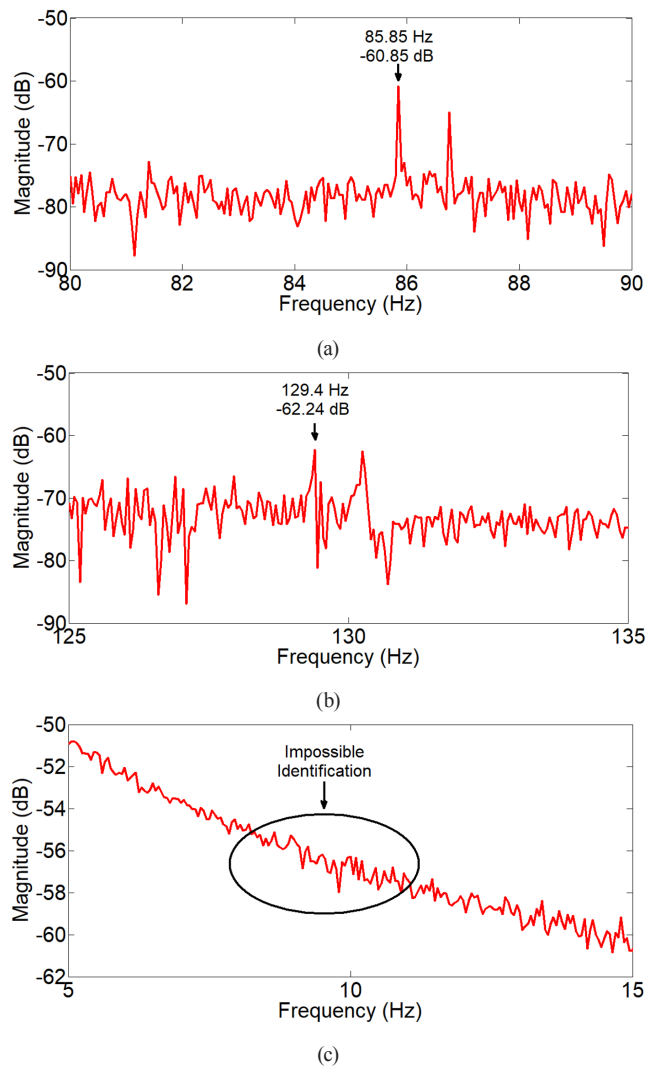


Fig. 7 Vibration spectrum according to all analyzed frequency bands – healthy bearings – (a) [80 Hz–90 Hz], (b) [125 Hz–135 Hz], (c) [5 Hz–15 Hz]

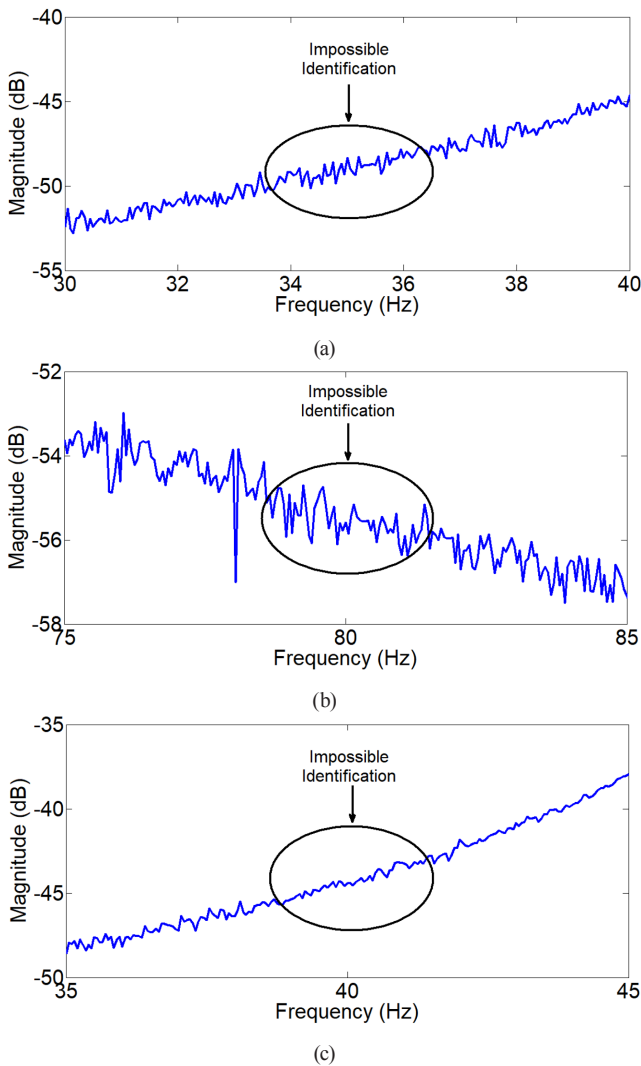


Fig. 8 Stator current spectrum according to all analyzed frequency bands – healthy bearings – (a) [30 Hz–40 Hz], (b) [75 Hz–85 Hz], (c) [35 Hz–45 Hz]

appears on the frequency band [5 Hz–15 Hz], thus indicating the absence of a cage fault.

- For the current technique: according to Fig. 8, no frequency signature appears on the three frequency bands analyzed [30 Hz–40 Hz], [75 Hz–85 Hz] and [35 Hz–45 Hz].

4.3 Operating mode with an outer race fault

In this operating mode, the tested bearing has a 3 mm hole on the outer race. Fig. 9 represents both vibration and the stator current spectrums obtained using the PSD estimation by the Periodogram technique.

According to Fig. 9 (a) and (b), and also Table 1, the outer race fault signature is clearly detectable on both spectrums: vibration and stator current. Furthermore,

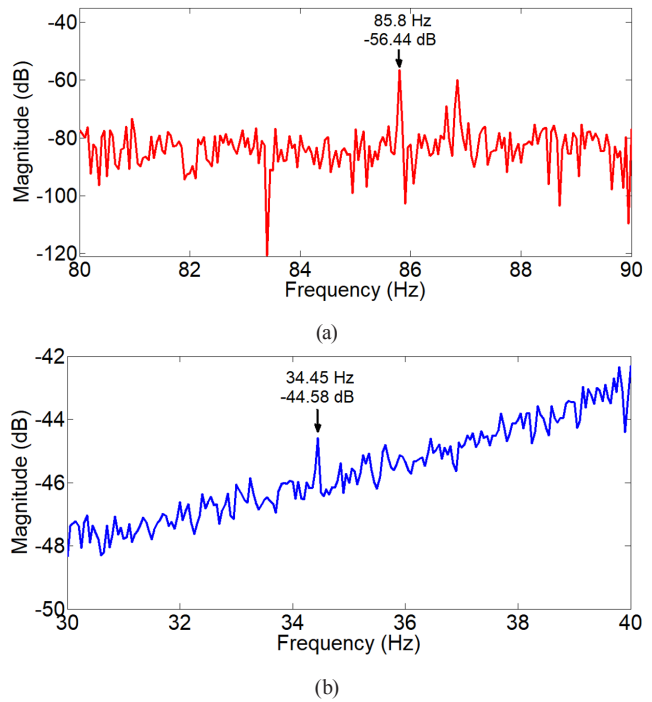


Fig. 9 Spectrum of vibration and stator current – Outer race fault – (a) Vibration technique, (b) Stator current technique

a comparison of the results displayed in Fig. 7 (a) and Fig. 9 (a), shows an increase in the amplitude of the harmonic of the outer race fault (85.8 Hz / -56.44 dB) compared to the healthy case (85.85 Hz / -60.85 dB). This is an indicator of the fault severity.

On the other hand, on the current spectrum, the fault signature is detectable compared to the healthy case (see Fig. 8 (a) and Fig. 9 (b)). Therefore, Table 2 summarizes the theoretical frequencies and the real frequencies obtained for an outer race fault from the spectrum of vibration and stator current.

The slight difference between the mentioned frequencies in Table 2 is completely normal because of the frequency resolution used and the error in the measurement of the rotation speed. The obtained results show the superiority of the vibration technique in detecting and monitoring the outer race fault signature compared to the stator current technique.

Table 2 Outer race fault signature obtained by the vibration technique and the stator current technique

Technique	Theoretical frequency	Healthy bearing	Outer race fault
Vibration	85.73 Hz	85.85 Hz -60.85 dB	85.5 Hz -56.44 dB
Stator current	35.73 Hz	Doesn't exist	34.45 Hz -44.58 dB

4.4 Motor operating with an inner race fault

An inner race with a 3 mm hole is used in this operating mode. Fig. 10 represents the vibration and stator current spectrum obtained using the PSD estimation by Periodogram.

According to Fig. 10 (a), the vibration spectrum shows the inner race fault signature (129.2 Hz / -41.91 dB). This signature increased compared to the healthy case (129.4 Hz / -62.24 dB. see Fig. 7 (b)), thus indicating that the fault severity is more important. Regarding the current technique, no frequency signature is detected on the frequency band (Fig. 10 (b)), despite the existence of the inner race fault. Table 3 summarizes the frequency signatures of this fault for both studied techniques.

The obtained results show once again the superiority of the vibration technique in the detection of the inner race fault compared to the stator current technique.

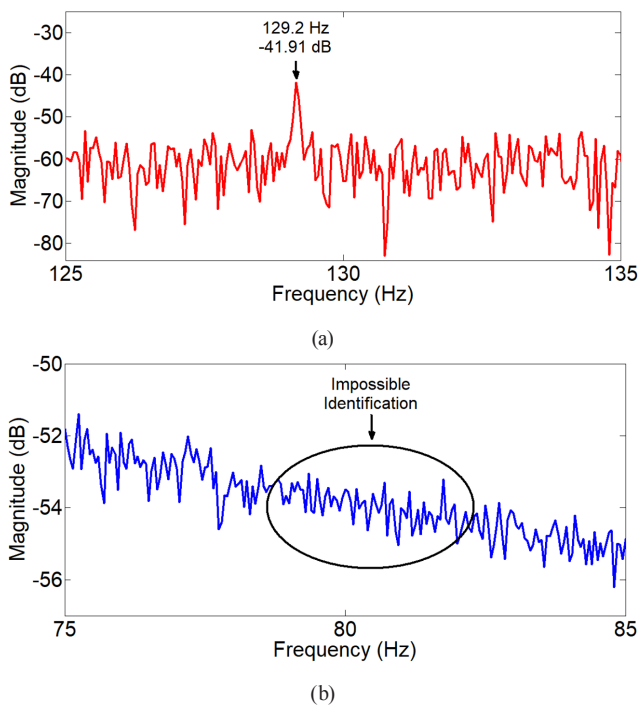


Fig. 10 Spectrum of vibration and stator current – Inner race fault – (a) Vibration technique, (b) Stator current technique

Table 3 Inner race fault signature obtained by the vibration technique and the stator current technique

Technique	Theoretical frequency	Healthy bearing	Outer race fault
Vibration	130.26 Hz	129.4 Hz -62.24 dB	129.2 Hz -41.91 dB
Stator current	80.86 Hz	Doesn't exist	Doesn't exist

4.5 Motor operating with a cage fault

In the last operating mode, a hole is created in the cage of bearing. The vibration and stator current spectrum obtained using the PSD estimation by Periodogram are illustrated in Fig. 11 (a) and (b) respectively.

According to Fig. 11 (a), the frequency signature of the cage fault is not detectable by the vibration technique. On the other hand, the stator current analysis makes it possible to detect a signature at the frequency 40 Hz with an amplitude of -51.63 dB. This signature corresponds the cage fault according to Table 1. The slight difference between the value of this real frequency 40 Hz and that theoretical 40.48 Hz is completely normal considering the error on the measurement of the rotation speed. This test proves that the stator current analysis gives better results than the vibration technique in the detection of the cage fault.

In light of the obtained results, we can say that the vibration analysis is more efficient in detecting the inner and outer race faults. However, it is advisable to use the stator current technique in detecting the cage fault. This shows that both analysis techniques are complementary.

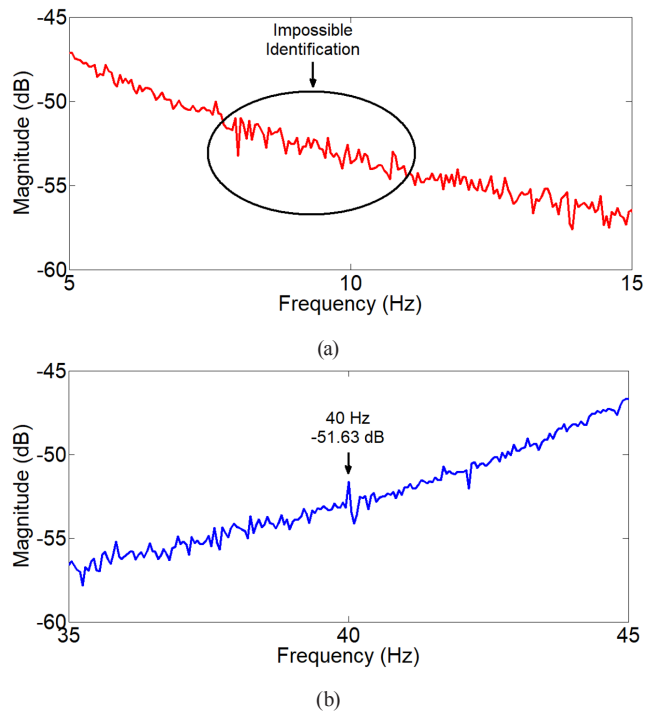


Fig. 11 Spectrum of vibration and stator current – cage fault – (a) Vibration technique, (b) Stator current technique

5 Conclusions

In this paper, rolling element bearing fault diagnosis of induction motor is carried out using the vibration technique and the stator current technique in order to compare the performance of both techniques. The experimental results obtained show that the vibration analysis is more efficient in detecting inner and outer race faults. On the other hand, the stator current analysis is more reliable in detecting cage faults, which proves the complementarity of both techniques.

References

- [1] Toliyat, H. A., Nandi, S., Choi, S., Meshgin-Kelk, H. "Electric Machines: Modeling, Condition Monitoring, and Fault Diagnosis", CRC Press, Boca Raton, FL, USA, 2013.
- [2] Thorsen, O. V., Dalva, M. "Failure identification and analysis for high-voltage induction motors in the petrochemical industry", IEEE Transactions on Industry Applications, 35(4), pp. 810–818, 1999.
<https://doi.org/10.1109/28.777188>
- [3] Bonnett, A. H., Yung, C. "Increased Efficiency Versus Increased Reliability", IEEE Industry Applications Magazine, 14(1), pp. 29–36, 2008.
<https://doi.org/10.1109/MIA.2007.909802>
- [4] McNerny, S. A., Dai, Y. "Basic vibration signal processing for bearing fault detection", IEEE Transactions on Education, 46(1), pp. 149–156, 2003.
<https://doi.org/10.1109/TE.2002.808234>
- [5] Immovilli, F., Bellini, A., Rubini, R., Tassoni, C. "Diagnosis of Bearing Faults in Induction Machines by Vibration or Current Signals: A Critical Comparison", IEEE Transactions on Industry Applications, 46(4), pp. 1350–1359, 2010.
<https://doi.org/10.1109/tia.2010.2049623>
- [6] Henriquez, P., Alonso, J. B., Ferrer, M. A., Travieso, C. M. "Review of Automatic Fault Diagnosis Systems Using Audio and Vibration Signals", IEEE Transactions on Systems, Man, and Cybernetics: Systems, 44(5), pp. 642–652, 2014.
<https://doi.org/10.1109/TSMCC.2013.2257752>
- [7] Zarei, J., Tajeddini, M. A., Karimi, H. R. "Vibration analysis for bearing fault detection and classification using an intelligent filter", Mechatronics, 24(2), pp. 151–157, 2014.
<https://doi.org/10.1016/j.mechatronics.2014.01.003>
- [8] Sun, L., Xu, B. "An Improvement of Stator Current Based Detection of Bearing Fault in Induction Motors", In: 2007 IEEE Industry Applications Annual Meeting, New Orleans, LA, USA, 2007, pp. 2277–2281.
<https://doi.org/10.1109/07ias.2007.344>
- [9] Blodt, M., Granjon, P., Raison, B., Rostaing, G. "Models for Bearing Damage Detection in Induction Motors Using Stator Current Monitoring", IEEE Transactions on Industrial Electronics, 55(4), pp. 1813–1822, 2008.
<https://doi.org/10.1109/TIE.2008.917108>
- [10] Elbouchikhi, E., Choqueuse, V., Amirat, Y., Benbouzid, M. E. H., Turri, S. "An Efficient Hilbert–Huang Transform-Based Bearing Faults Detection in Induction Machines", IEEE Transactions on Energy Conversion, 32(2), pp. 401–413, 2017.
<https://doi.org/10.1109/TEC.2017.2661541>
- [11] Koura, M. B., Boudinar, A. H., Aimer, A. F. "Improved Diagnosis of Induction Motor's Rotor Faults using the Papoulis Window", In: 2019 International Aegean Conference on Electrical Machines and Power Electronics (ACEMP) & 2019 International Conference on Optimization of Electrical and Electronic Equipment (OPTIM), Istanbul, Turkey, 2019, pp. 216–220.
<https://doi.org/10.1109/ACEMP-OPTIM44294.2019.9007131>
- [12] Gherabi, Z., Benouzza, N., Toumi, D., Bendiabdellah, A. "Eccentricity Fault diagnosis in PMSM using Motor Current Signature Analysis", In: 2019 International Aegean Conference on Electrical Machines and Power Electronics (ACEMP) & 2019 International Conference on Optimization of Electrical and Electronic Equipment (OPTIM), Istanbul, Turkey, 2019, pp. 205–210.
<https://doi.org/10.1109/ACEMP-OPTIM44294.2019.9007164>
- [13] Stack, J. R., Harley, R. G., Habetler, T. G. "An amplitude Modulation detector for fault diagnosis in rolling element bearings", IEEE Transactions on Industrial Electronics, 51(5), pp. 1097–1102, 2004.
<https://doi.org/10.1109/TIE.2004.834971>
- [14] Obaid, R. R., Habetler, T. G., Stack, J. R. "Stator current analysis for bearing damage detection in induction motors", In: 4th IEEE International Symposium on Diagnostics for Electric Machines, Power Electronics and Drives (SDMPED 2003), Atlanta, GA, USA, 2003, pp. 182–187.
<https://doi.org/10.1109/DEMPED.2003.1234570>
- [15] Aimer, A. F., Boudinar, A. H., Benouzza, N., Bendiabdellah, A. "Induction motor bearing faults diagnosis using Root-AR approach: simulation and experimental validation", Electrical Engineering, 100(3), pp. 1555–1564, 2018.
<https://doi.org/10.1007/s00202-017-0527-1>
- [16] Trajin, B., Regnier, J., Faucher, J. "Bearing fault indicator in induction machine using stator current spectral analysis", In: 4th IET International Conference on Power Electronics, Machines and Drives (PEMD 2008), York, UK, 2008, pp. 592–596.
<https://doi.org/10.1049/cp:20080590>
- [17] Boudinar, A. H., Benouzza, N., Bendiabdellah, A., Khodja, M. "Induction Motor Bearing Fault Analysis Using a Root-MUSIC Method", IEEE Transactions on Industry Applications, 52(5), pp. 3851–3860, 2016.
<https://doi.org/10.1109/TIA.2016.2581143>
- [18] Jung, J. H., Lee, J. J., Kwon, B. H. "Online Diagnosis of Induction Motors Using MCSA", IEEE Transactions on Industrial Electronics, 53(6), pp. 1842–1852, 2006.
<https://doi.org/10.1109/TIE.2006.885131>

Acknowledgement

Authors would like to thank all the members of the Laboratory of Development of Electric Drives of the University of Sciences and Technology of Oran - Mohamed Boudiaf, USTO-MB, ALGERIA, for the help they brought to the experimental validation of this work.

- [19] Schoen, R. R., Habetler, T. G., Kamran, F., Bartfield, R. G. "Motor bearing damage detection using stator current monitoring", IEEE Transactions on Industry Applications, 31(6), pp. 1274–1279, 1995. <https://doi.org/10.1109/28.475697>
- [20] Schoen, R. R., Habetler, T. G. "A New Method of Current-based Condition Monitoring in Induction Machines Operating Under Arbitrary Load Conditions", Electric Machines & Power Systems, 25(2), pp. 141–152, 1997. <https://doi.org/10.1080/07313569708955729>
- [21] Bendiabdellah, A., Boudinar, A. H., Benouzza, N., Khodja, M. "The enhancements of broken bar fault detection in induction motors", In: 2015 International Aegean Conference on Electrical Machines & Power Electronics (ACEMP), 2015 International Conference on Optimization of Electrical & Electronic Equipment (OPTIM) & 2015 International Symposium on Advanced Electromechanical Motion Systems (ELECTROMOTION), Side, Turkey, 2015, pp. 81–86. <https://doi.org/10.1109/OPTIM.2015.7426972>

Appendix

Geometric parameters of the bearing 6205-ZZ:

- | | | | |
|-----------------------|---------|-------------------|----------|
| • Outer race diameter | 52 mm | • Ball diameter | 7.938 mm |
| • Inner race diameter | 25 mm | • Number of balls | 9 |
| • Cage diameter | 38.5 mm | • Contact angle | 0. |